

FEM-Based Numerical Analysis of the Laser Welding of Air Conditioner Components

Abstract: The article presents the FEM-based numerical model of the laser beam welding process. The modelling aimed to identify the effect of technological conditions of the laser welding of elements on the heating dynamics and the maximum temperature of elements being joined. The numerical modelling was performed using the SYSWELD software programme. The elements to be joined were a connector and a ring-like crimped conduit made of corrosion resistant steel grade 316L and 304.

Keywords: laser welding, numerical modelling, FEM, air conditioners, steel grade 316L, steel grade 304

DOI: [10.17729/ebis.2018.3/6](https://doi.org/10.17729/ebis.2018.3/6)

Introduction

Presently performed research works aim to develop new material-structural solutions in relation to car air-conditioning equipment based on the use of alternative coolant R744 (CO₂). The scope of research-related tests includes the selection of materials, the development of technologies enabling the making of products out of previously selected materials, the development of technologies making it possible to join individual components and of techniques ensuring the sealing of joined components. The aforesaid research scope also involves the selection of an optimum design of a device in terms of heat exchange, corrosion resistance as well as static and fatigue strength. Solutions and technologies to be developed will find applications in components of air-conditioners

as conduits enabling the transfer of a coolant (air-conditioning conduits). In particular, the above-named components will include metal tubes, flexible rubber hoses, fasteners and separable elements, joint gaskets and coolant storage containers. The necessity of undertaking the aforementioned (material-structural-related) research results from above-standard thermodynamic operation parameters of medium R744 in air-conditioners. In comparison with presently used R1234yf or disused R134a, the operating pressure of medium R744 in an air-conditioner is approximately 10 times higher (standards operating pressure of R744 amounts to 130 bar, whereas its momentary values may reach as many as 160 bar). In addition, the operating temperature of R744 is also significantly higher and amounts to 150°C.

mgr inż. Janusz Piłkuła (MSc Eng.), dr inż. Marek Węglowski (PhD (DSc) Eng.) – Instytut Spawalnictwa, Testing of Materials Weldability and Welded Constructions Department; mgr inż. Jerzy Dworak (MSc Eng.) – Instytut Spawalnictwa, Welding Technologies Department; Grzegorz Ziobro, Adam Szafron – Maflow Member of Boryszew Group, Tychy

The primary issue in performed tests was the selection of appropriate and applicable aluminium grades, corrosion resistant steels and auxiliary materials (e.g. soldering/brazing filler metals, gaskets etc.). The selection of optimum material solutions will be possible on the basis of tests aimed to characterise selected material properties, including mechanical strength, corrosion resistance, heat resistance and fatigue strength. One of the most important issues was to develop a laser welding technology enabling the obtainment of high-quality joints. One of the major challenges when welding small-sized and thin-walled elements is the melting of such elements without affecting their metallic continuity as, in cases of high operating pressure and fatigue loads, the failure to maintain the above-named material continuity can result in damage to elements during their operation. For this reason, it is important to know the field of temperature during welding. The knowledge of the above-named temperature field enables the determination of temperature changes (if any) in crucial areas. The aforesaid changes in temperature might lead to the formation of an unfavourable microstructure in the material, potentially weakening the entire structure. As the performance of actual welding tests and related testing of joints is both time-consuming and costly, the solving of the above-presented technical problems is often aided using numerical methods, e.g. the Finite Element Method (FEM) [1-3]. This article presents an FEM-based numerical model of laser beam welding. The

modelling aimed to identify the effect of laser welding technological conditions on heating dynamics and the maximum temperature of elements being joined. The numerical modelling was performed using a SYSWELD software programme. Elements subjected to the tests were a connector and a ring-like crimped conduit (Fig. 1) made of corrosion resistant steel 316L.

World-wide available reference publications contain numerous results of both actually performed Nd:YAG laser welding tests and results of tests performed using numerical (primarily FEM-based) methods. Publication [4] presents numerical analysis including thermal and elastoplastic phenomena accompanying Nd:YAG laser welding. Elements subjected to welding were plates made of corrosion resistant steel 316L. The authors performed tests of three commonly used heat sources when modelling laser welding processes, i.e. a truncated cone, a truncated cone and a double ellipsis as well as a double ellipsis and a truncated cone and a cylinder. The validation of developed models indicated appropriate conformity of temperature calculation results, residual stresses and welding strains with measurements of actual elements. The results revealed that the test results most consistent with the actual process were obtained using the model involving the heat source in the form of a truncated cone and a cylinder (Fig. 2).

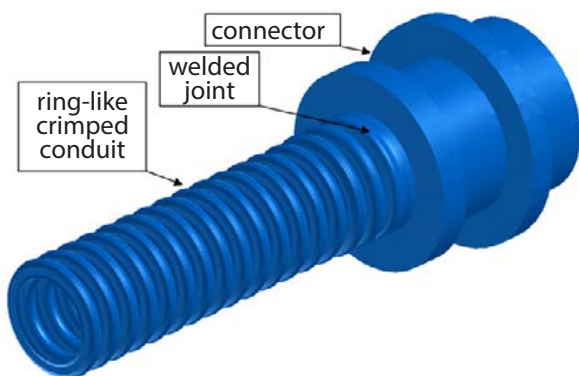


Fig. 1. Geometry of laser welded elements made in steel grade 316L

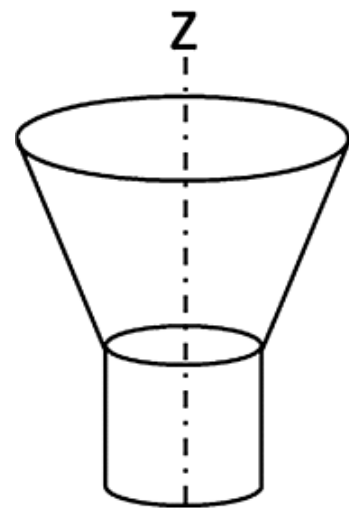


Fig. 2. Geometry of the heat source in the form of a truncated cone and a cylinder [4]

Publication [5] presents an FEM-based numerical model along with calculated strains generated during the laser welding of steel AH36 used in the ship-building industry. The authors indicated the very high conformity of results calculated using the FEM-based numerical model with those measured in relation to actual elements. The model was developed and related calculations were performed using the SYSWELD software programme. Article [6] presents results of numerical simulation of Nd:YAG laser welding. Elements subjected to welding were thin sheets made of steel grade DP600. The model involved the use of material properties in the function of temperature, allowing for phase transformations of the material. The authors indicated the very high conformity of computational results with those measured in relation to actual elements. Article [7] was concerned with tests related to laser and hybrid welding. The tests aimed to identify the field of temperature in elements subjected to welding as well as the flow of liquids in the material melting area. The model involved equations describing the transport of heat in the transient state and the Navier-Stokes equation. Article [8] presents the numerical analysis of laser welding based on equations describing the mechanics of continuous media as well as classical Johnson-Mehl-Avrami (JMA) and Koistinen-Marburger (KM) kinetic models including phase transformations in steel grade S460.

Actual Nd:YAG laser welding process

The technological tests of the welding process performed using the Nd-YAG laser beam emitted in a pulsed mode involved the use of a TruLaser Station 5004 device. The fastener was fixed in a three-clamp holder of numerical controller welding positioner synchronised with the TruLaser Station 5004 device control system. In turn, the hose was placed (using the welding positioner) in accordance with the axis of rotation and subjected to slight pressure aimed to eliminate a gap between the elements.

The elements were not tack-welded before welding proper. During the welding process, temperature on the specimen surface was measured using thermocouples (Fig. 3).

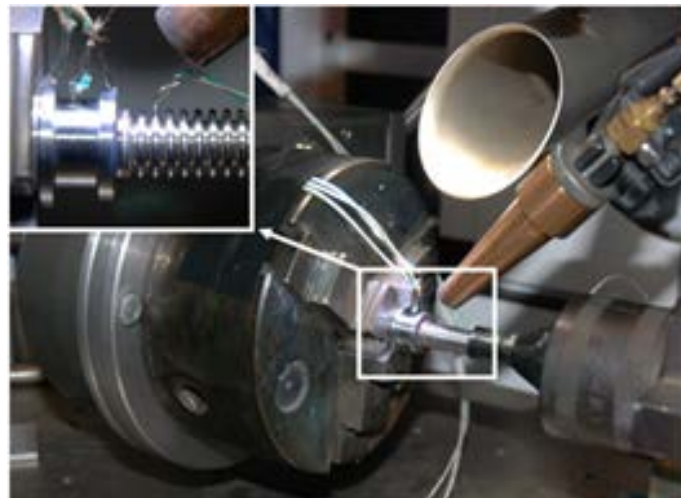


Fig. 3. Test rig for Nd-YAG laser beam welding

The laser welding test was performed using the following parameters:

- impulse shape – CrNi type (Fig. 4),
- maximum impulse shape: $P = 1000$ W,
- impulse duration (time): $t = 4$ ms,
- laser beam diameter: $d = 0.6$ mm,
- workpiece rate of rotation: $n = 4$ rpm (linear welding rate: 2.041 mm/s),
- impulse (repetition) frequency: $f = 10.45$ Hz, laser beam focus position: interface of the elements being joined,
- shielding gas: Ar, 7 l/min, side nozzle.

The girth weld was made using one entire turn and an overlap of 40° .

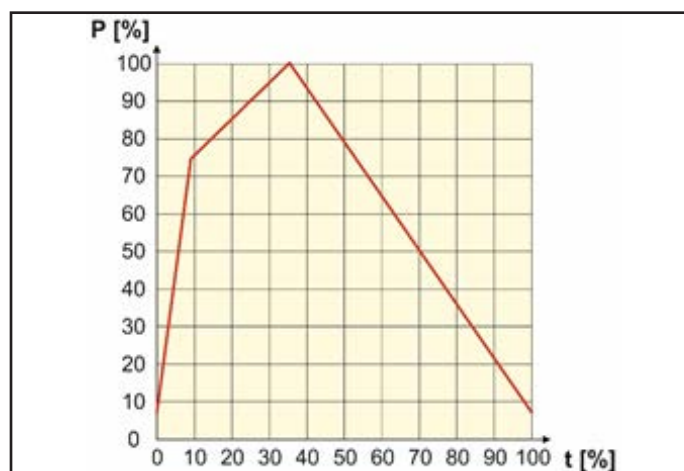


Fig. 4. Changes in laser radiation beam power in time in relation to the CrNi type impulse

In the pulsed mode, the emission of YAG laser beam radiation results from the impulse excitation of the laser resonator. The above-named excitation is performed through optical pumping, i.e. the lighting of the resonator with impulses of radiation generated by laser diodes grouped in so-called packages (i.e. modules containing a specific number of diodes). The operation of YAG crystalline lasers is characterised by the generation of the significant amount of heat by pumping modules. The foregoing limits the maximum average power and energy of a radiation beam impulse (primary parameters of pulsed laser operation). The energy of an impulse depends on the combination of its power and width (i.e. duration). The above-named radiation beam parameters cannot be shaped freely. This means that it is not possible to freely determine the duration of an impulse and the frequency of its emission in relation to assumed average power of the radiation beam (Fig. 5). In relation to each resonator, the energy of an impulse cannot exceed a specific maximum value. As regards impulse operation, average laser radiation power P_a is defined as the product of the average radiation power of one impulse P_i , the duration of one impulse t_i and the number of impulses per one second expressed through the frequency of emission f (1). In relation to specific power there are a number of combinations in terms of the adjustment of impulse energy and the frequency of impulse repetition.

$$P_a = P_i \cdot t_i \cdot f = E_i \cdot f \quad (1)$$

The impulse emission frequency is strictly related to the period of their occurrence expressed by the following correlation (2):

$$T = \frac{1}{f} \quad (2)$$

The average energy of laser radiation in relation to the impulse operation mode is defined as the product of the average radiation power and the laser beam effect duration (3):

$$E_a = P_a \cdot t \quad (3)$$

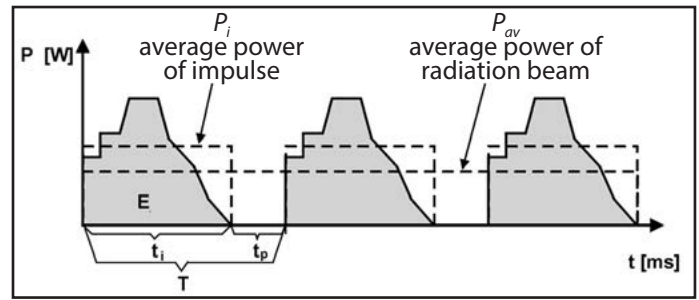


Fig. 5. Graphic interpretation: impulse average power P_i , radiation beam average power P_{av} , impulse energy E_i , impulse width t_i , pause time t_p and impulse period T

The weld obtained in the process of welding involving the use of a laser beam emitted in the pulsed mode is composed of a number of overlapping spot welds. The degree of the overlapping of individual impulses expressed in percentage (the so-called overlap) indicates to what extent the area of the material melted by a single impulse overlaps with a similar area made by the previous impulse (Fig. 6). By changing the overlap width it is possible to adjust a heat input to the material being welded as well as affect the homogeneity of the weld structure. The overlap is determined by a welding rate adjusted in accordance with the frequency of impulses. In turn, the frequency of impulses depends on the power of an impulse and its duration. If, because of a specific welding rate, an area melted by a single laser beam impulse adopts an elliptic shape, the longer axis of the ellipsis constitutes dimension S , whereas the shorter axis of the ellipsis constitutes dimension D (Fig. 7).

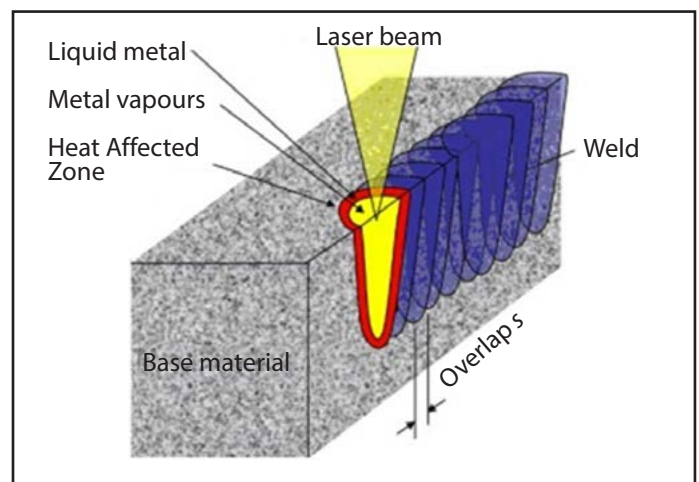


Fig. 6. Schematic laser welding process involving the use of the beam emitted in the pulsed mode

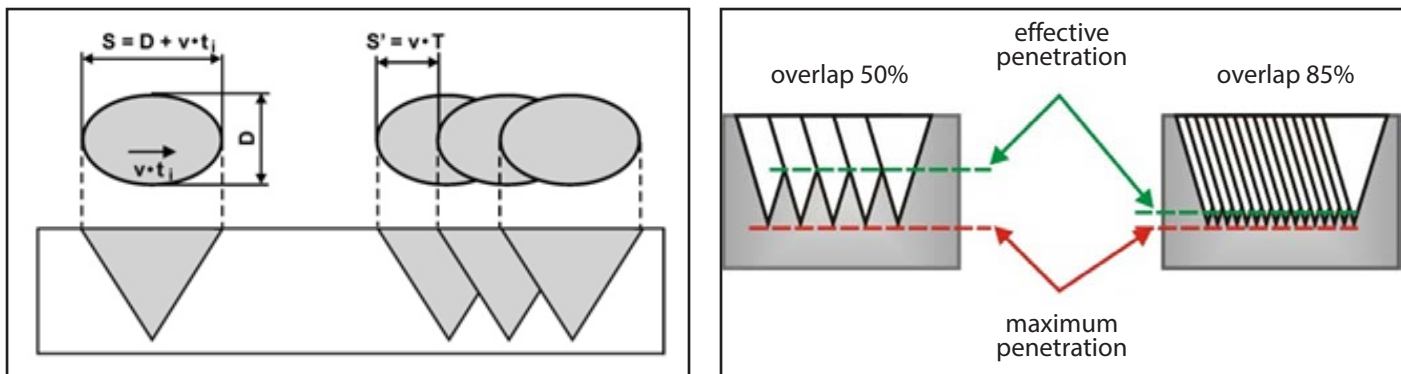


Fig. 7. Graphic interpretation of the overlap of laser beam impulses: v – welding rate, t_i – impulse duration (time), D – diameter of laser beam focused area, T – period of impulses

The degree of the overlapping of impulses (overlap) is expressed by the following dependence:

$$Z = \frac{S - S'}{S} \cdot 100\% \quad (4)$$

where

$$S = D + v \cdot t_i \quad (5),$$

$$S' = v \cdot T \quad (6).$$

After transforming dependences 4, 5 and 6, overlap Z amount to:

$$Z = \left(1 - \frac{v \cdot T}{D + v \cdot t_i} \right) \cdot 100\% \quad (7).$$

Overlap Z determines the effective depth of penetration (Fig. 7), yet it does not enable the determination of the effective and maximum penetration.

Numerical model of the Nd:YAG laser welding process

The mesh of finite elements in the FEM-based numerical model (Fig. 8) was based on the geometry of an actual element. The greatest length of the finite element side amounted to 1.4 mm. Because of the high gradient of temperature in the weld area and in the HAZ as well as due to the dimensions of the weld area, the mesh was consolidated and the length of the element side amounted to approximately 0.45 mm.

The mesh in the joint area and a fragment of the hose were made of solids. To limit the number of elements and, as a result, to reduce

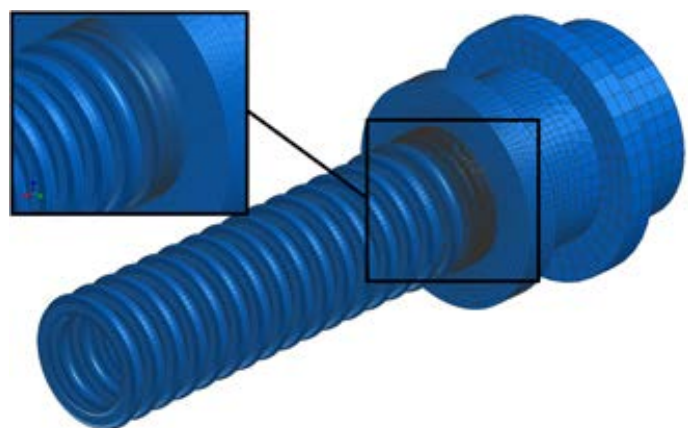


Fig. 8. Mesh of finite elements used in the FEM-based modelling of the Nd:YAG laser welding process

the time of calculations, at a further distance from the weld the mesh of the hose area was made of hull elements. Elements to be joined were a connector and a ring-like crimped hose made of corrosion resistant steels 316L and 304. The model included the following steel material properties in the function of temperature: specific heat, thermal conductivity and density (Fig. 9 and 10) [9].

The FEM model allowed for the exchange of heat with the environment, including the process of heat radiation and convection. The calculation of the amount of heat emitted by the body was based on the Stefan-Boltzmann law (11) taking into consideration surface emissivity coefficient ϵ as well as the difference between body temperature T and the temperature of environment T_0 .

$$q_s = \epsilon \cdot \sigma \cdot (T^4 - T_0^4) \quad (8),$$

where σ – black surface radiation constant, $5.67 \times 10^{-8} \text{ kg/s}^3\text{K}^4$.

Equation (1) was transformed in the calculations in order to determine heat exchange coefficient as resulting from the phenomenon of heat radiation (9) [10,11].

$$\alpha_r = \varepsilon \cdot \sigma \cdot (T + T_0) \cdot (T^2 + T_0^2) \tag{9}$$

The model involved the adoption of the emissivity coefficient amounting to 0.5 in relation to the surface outside the welded joint area and

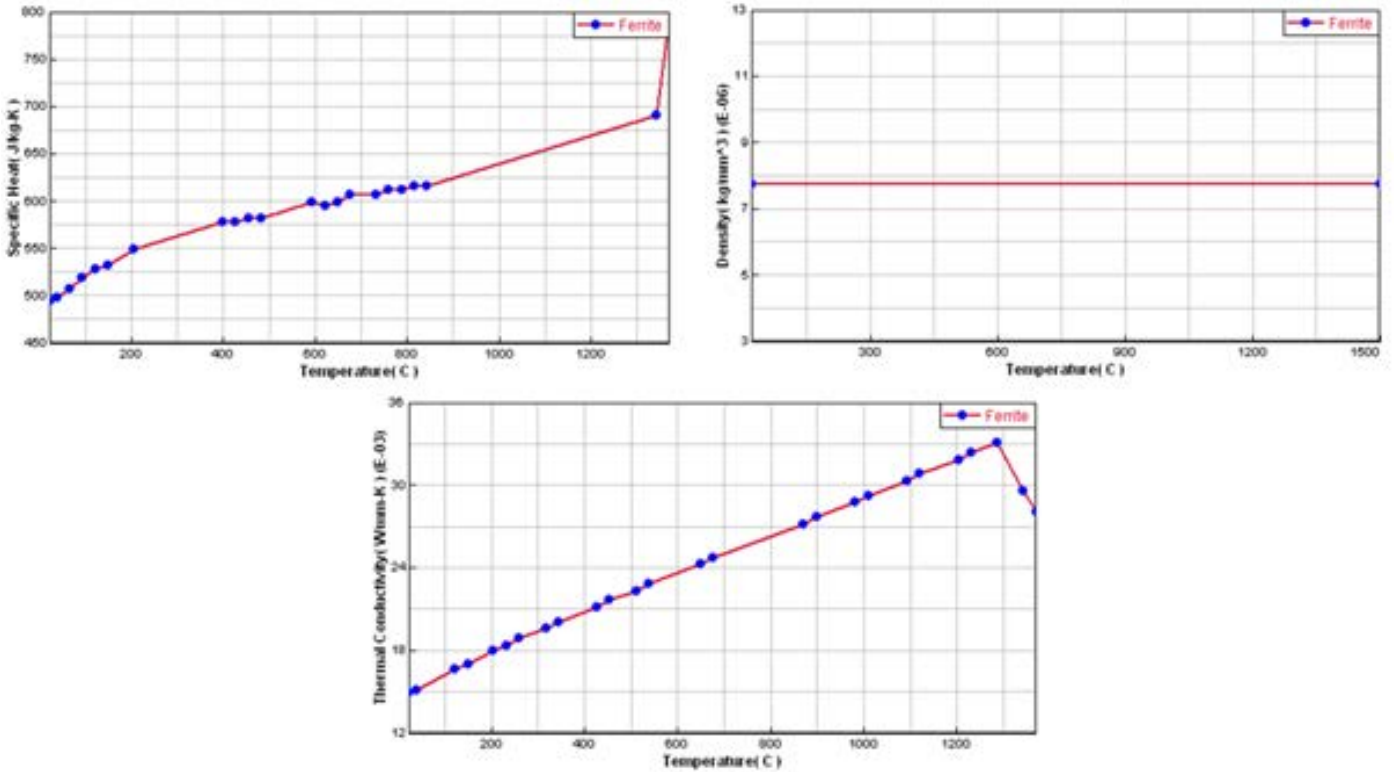


Fig. 9. Values of material properties in the function of the temperature of steel grade 316L: specific heat, density and thermal conductivity [9]

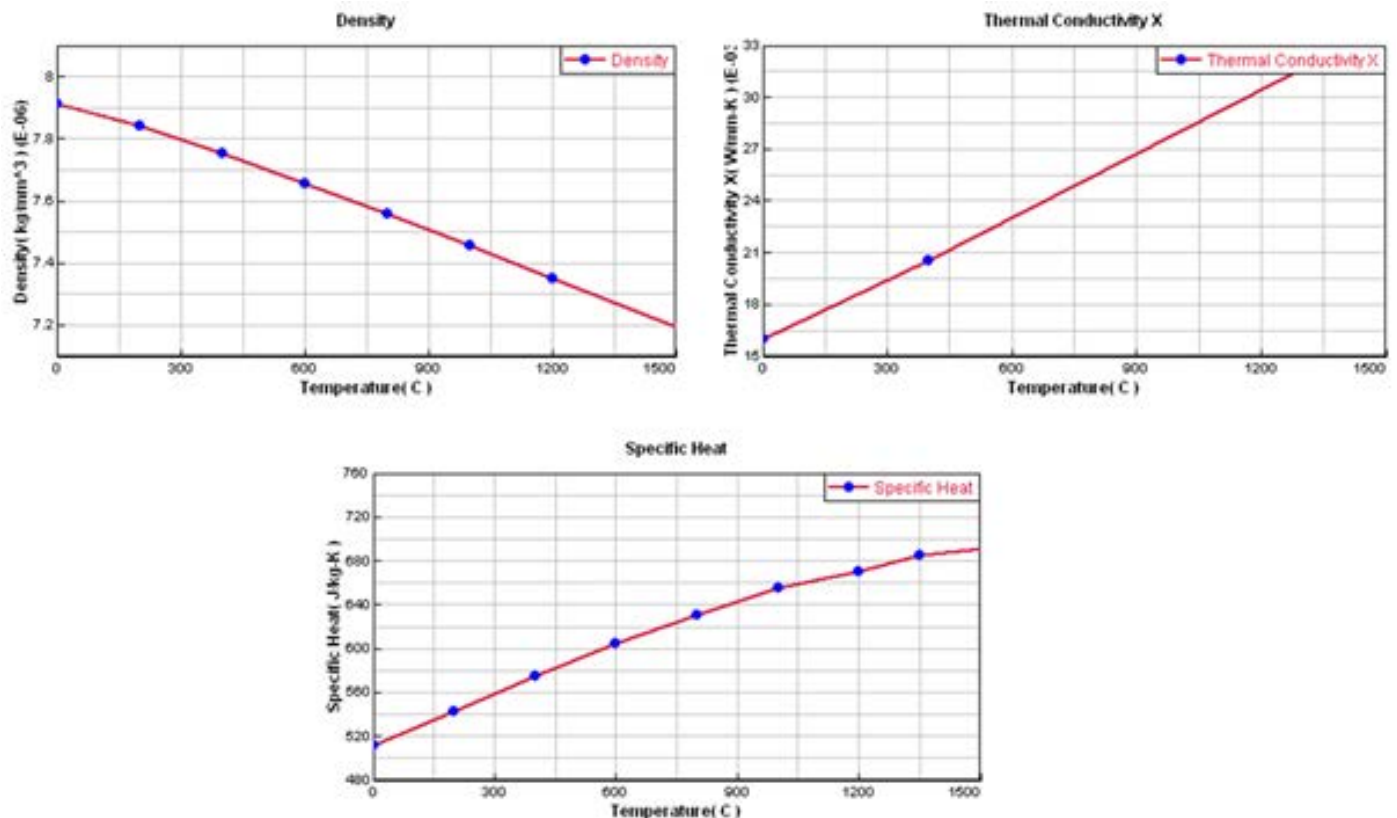


Fig. 10. Values of material properties in the function of the temperature of steel grade 304: density, thermal conductivity and specific heat [9]

0.8 in relation to the surface of the welded joint area. Non-dimensional heat exchange coefficient Nu (as a result of forced convection) was calculated on the basis of criterion equation (10):

$$Nu = C \cdot Re_a \cdot Pr^b \quad (10)$$

Reynolds number Re as non-dimensional velocity used to forecast similar flow schemes in various fluid flow situations was determined using equation (11), whereas Prandtl number Pr used as the primary criterion of fluid motion stability was determined using equation (12). Values of coefficients C , a , b in relation to the flow perpendicular to the tube amounted to 0.26, 0.6, and 0.3 respectively [12]. Shielding gas (argon) properties were obtained using the calculator of fluid properties [13]. Values adopted in relation to a constant temperature of 20°C were the following:

- specific heat $c=521.62 \text{ J/kgK}$,
- density $\rho=1.6617 \text{ kg/m}^3$,
- kinematic coefficient of viscosity $\nu=1.3416e-5 \text{ m}^2/\text{s}$,
- thermal conductivity coefficient $\lambda=0.017391 \text{ W/mK}$.
- shielding gas flow rate at the nozzle outlet amounted to 1.48 m/s.

$$Re = \frac{wL}{\nu} \quad (11)$$

$$Pr = \frac{c\rho\nu}{\lambda} \quad (12)$$

The heat exchange coefficient defined in the model and calculated using equation (13) amounted to 26.87 W/m²K.

$$\alpha = Nu \frac{\lambda}{L} \quad (13)$$

The value of the heat exchange coefficient in the presented model constituted the sum of calculated heat exchange coefficients resulting from heat radiation and convection (Fig. 11).

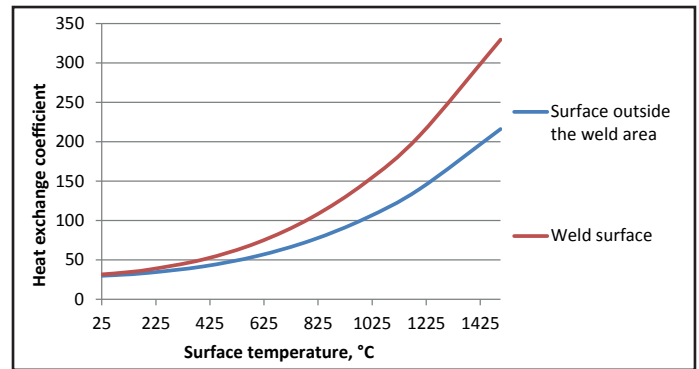


Fig. 11. Value of heat exchange coefficient α on the surface and outside the weld

The flow of heat is defined using the Fourier law, i.e. the principal law concerning quantitative conduction (14), whereas the transient process of heat flow in an isotropic medium in the presence of internal volumetric sources of heat is described by the Fourier equation (18).

$$q = -\lambda(T) \cdot gradT \quad (14)$$

$$c(T) \cdot \rho(T) \cdot \frac{\partial T}{\partial t} - div[\lambda(T) \cdot gradT] - Q = 0 \quad (15)$$

The formation of the weld pool during laser welding is a complex process. For this reason, engineering practice uses the simplified volumetric heat source based on the Gaussian distribution, in the form of a cylinder or a truncated cone [7, 8, 14, 15]. In the presented model, the heat source was described in the form of a truncated cone (Fig. 12), whereas the determination of the amount of energy was based on the actual welding process.

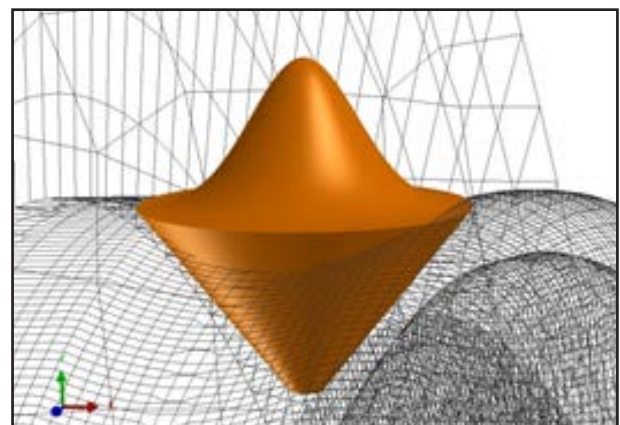


Fig. 12. Volumetric heat source (truncated cone) based on the Gaussian distribution

By contrast with the modelling of laser welding where the beam is emitted in a continuous or pulsed mode characterised by very high frequency, the modelling of pulsed laser welding having an impulse repetition frequency of 10.45 Hz required that each impulse be treated as a single weld. The duration of a single impulse amounted to approximately 0.004 s. Impulses (Fig. 4) occurred every 0.096 s. This means that at a linear rate of 2.041 mm/s, impulses occurred every 0.2 mm (Fig.13). The simulating of the above-named process as continuous welding (without impulses) involving the use of the same power of laser would result in a repeatedly higher heat input to the welding area, enabling the obtainment of the proper size of the weld. However, in the above-named case the field of temperature within the entire area subjected to analysis would be improper. Taking into consideration the average laser beam power would enable an appropriate heat input within entire welding time. However, power density in a time unit would be insufficient to obtain the proper geometry of the weld, or even to obtain temperature higher than the melting point of the material in the joint area. The modelling of the pulsed laser welding process characterised by the short duration of impulses and a welding rate leading to relatively long distances between successive impulses required treating each impulse as a separate joint, the formation of which was characterised by short duration, yet by the high density of energy.

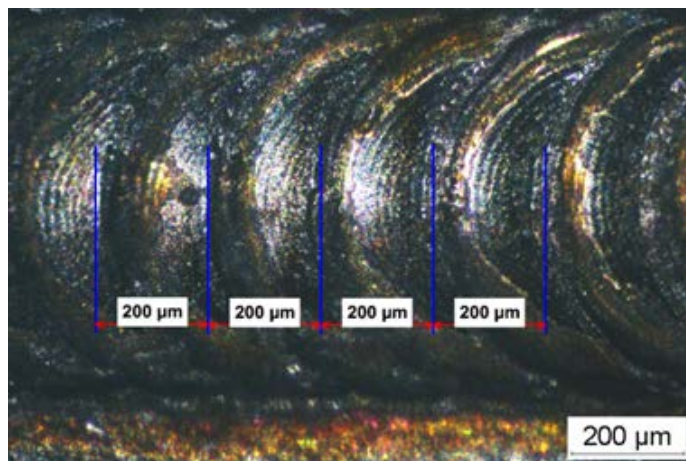


Fig. 13. Distance between successive impulses

The FEM-based model was validated on the basis of the dimensions of the actual weld and results obtained during temperature measurements at selected points of the elements being welded. The highest difference between the maximum temperature measured at the previously selected points (Fig. 14, 15) and the temperature measured using the FEM-based model amounted to 7.9 %. The average difference from all of the measurement points amounted to 3.9%. Taking into consideration the small dimensions of the elements subjected to welding and, as a result, the significant effect of geometry modelling imperfections (if any) on calculation results, welding process complexity and strongly non-linear transfer of heat to the environment (induced by the flow of the shielding gas), it can be stated that the temperature measurement results were consistent with those obtained in the actual tests.

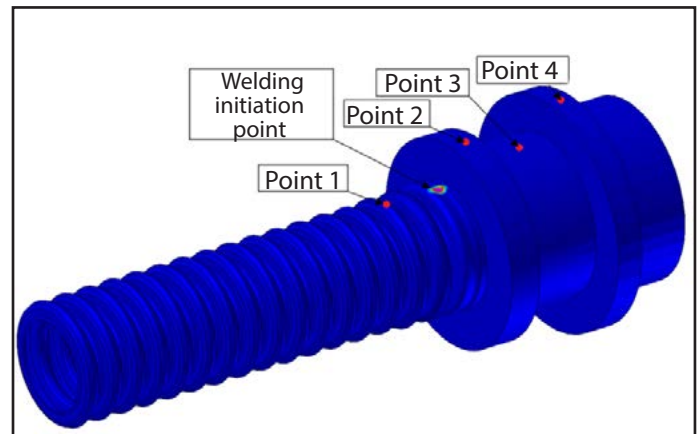


Fig. 14. Temperature measurement point during Nd:YAG laser beam welding

The geometry of the weld was determined on the basis of the melting point of steel 316L, restricted within the range of 1375°C to 1400°C [16]. The temperature field determined using the FEM-based model and the metallographic photograph revealed the conformity of the dimensions and the shape of the weld (Fig. 16). The analysis of numerical calculation results demonstrated the right choice as regards the use of the overlap as, at the initial stage, the weld was overly shallow and overly narrow to fit the required spring area (Fig. 17). The FEM-

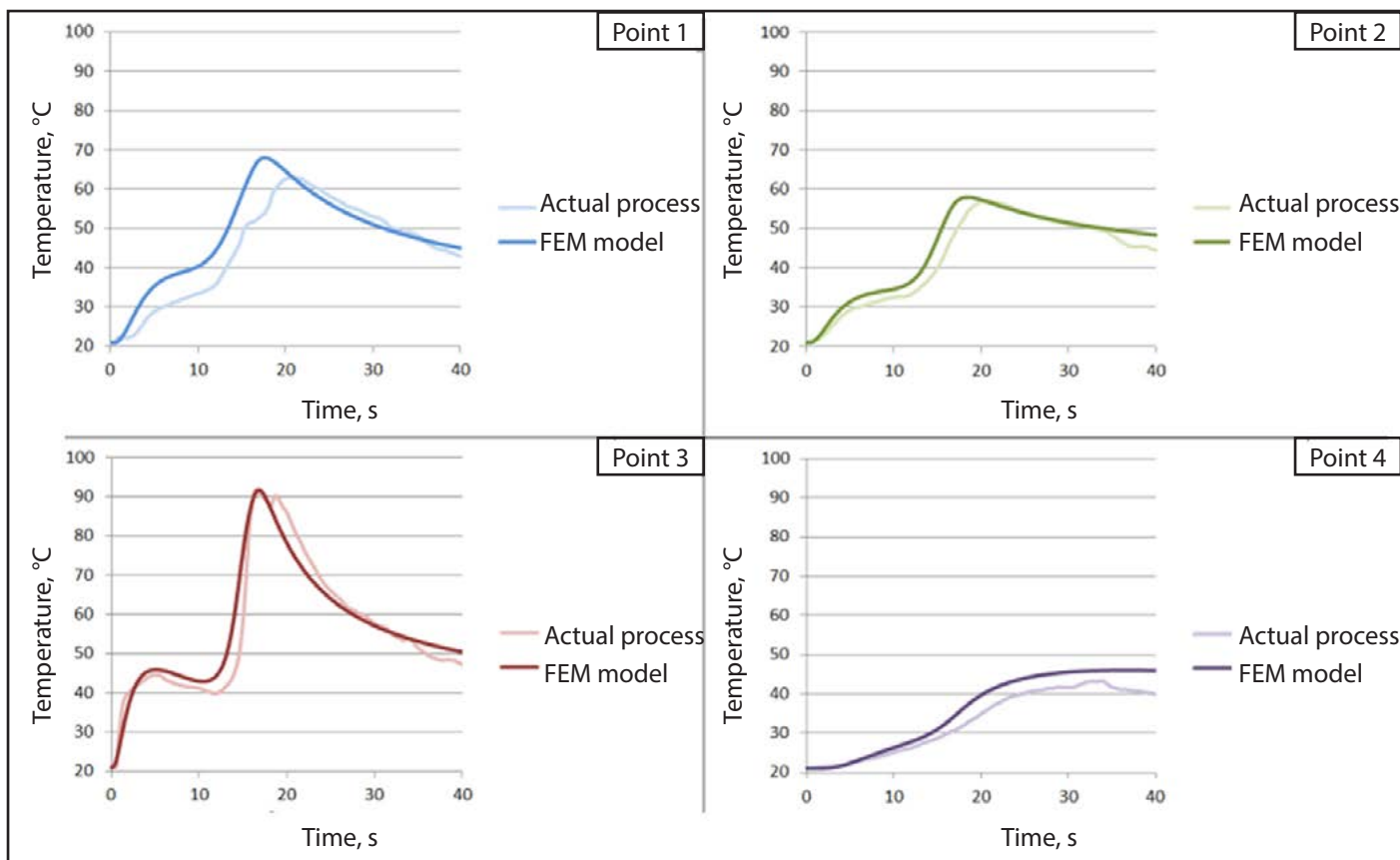


Fig. 15. Temperature measurement results in relation to the actual process and temperature calculated at selected points indicated in Figure 14

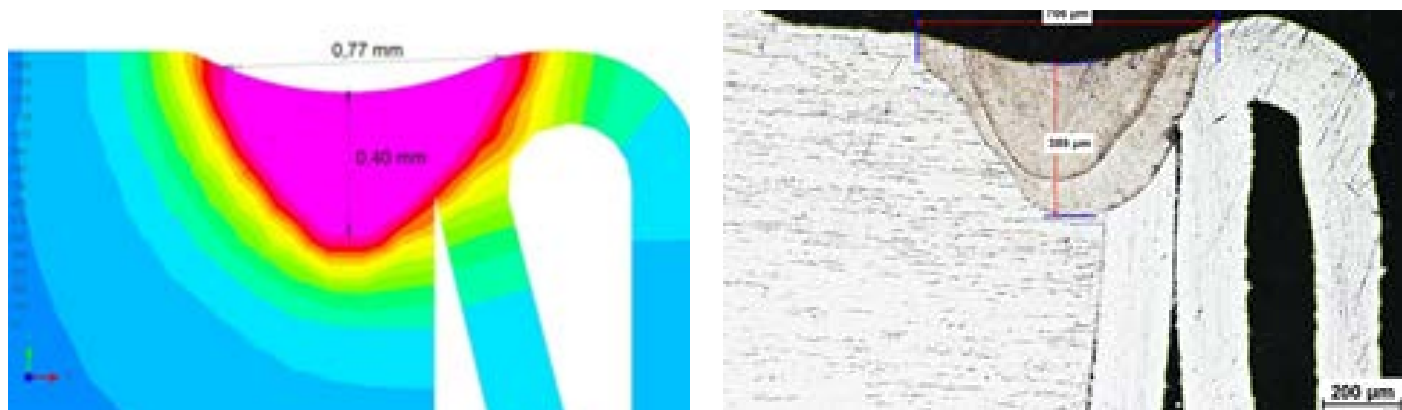


Fig. 16. Geometry and dimensions of the modelled (left) and actual (right) weld

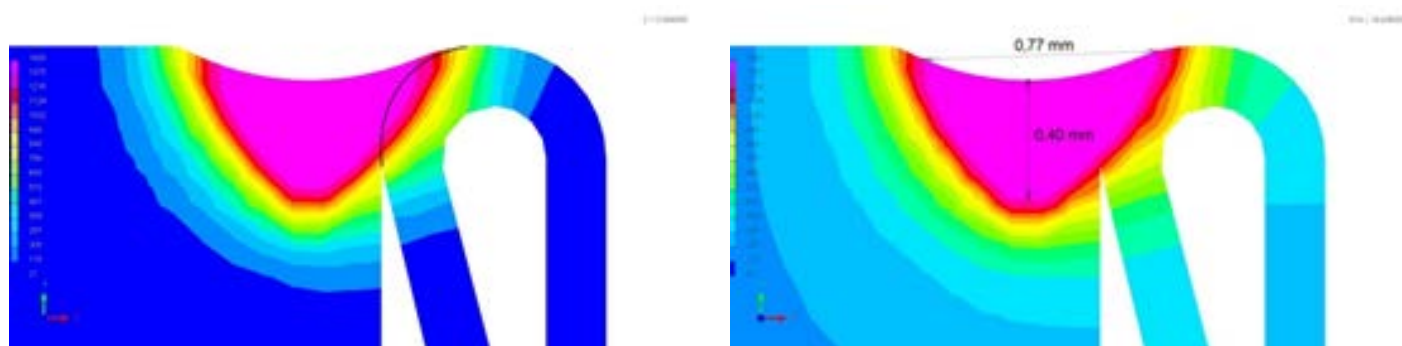


Fig. 17. Geometry of the weld at the welding process initiation point in relation to the process without the overlap (left) and after the use of the overlap (right)

-based simulation enabled the determination amounting to approximately 0.37 mm and of the effective and maximum penetration, 0.40 mm respectively (Fig. 18).

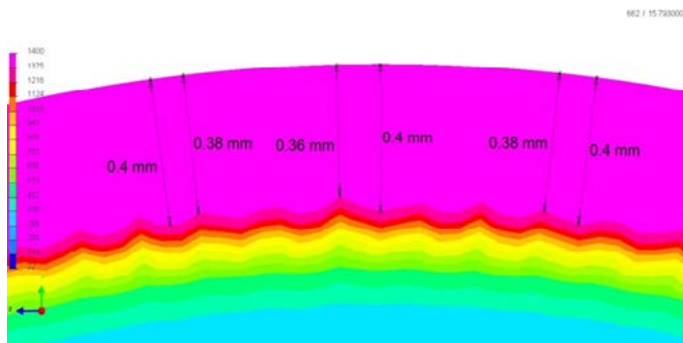


Fig. 18. Effective and maximum penetration in the Nd:YAG laser welded joint

Summary

The FEM-based numerical model of pulsed laser welding developed within the research work discussed in the article has proved consistent with the actual welding process as regards the field of temperature and the weld geometry. The possibility of obtaining FEM modelling-based information about the depth of penetration, temperature at selected crucial points as well as effective and maximum penetration indicates that the model will find application when developing the welding technology at further research stages. The modelling of the pulsed laser welding process characterised by the short duration of impulses and a welding rate leading to relatively long distances between successive impulses requires treating each impulse as a separate joint, the formation of which is characterised by a short duration and the high density of energy.

Acknowledgments

This work has been performed with funding from National Centre for Research and Development in Poland within the frame of the research grant no PBS3/B5/43/2015 entitled: "The choice of materials and the development of the construction elements of air conditioning elements designed to work with the new refrigerant R744".

References

- [1] Slováček M., Kik T.: *Use of Welding Process Numerical Analyses as Technical Support in Industry. Part 1: Introduction to Welding Process Numerical Simulations*. Biuletyn Instytutu Spawalnictwa, 2015, no. 4, pp. 25-31. <http://dx.doi.org/10.17729/ebis.2015.4/3>
- [2] Kik T., Slováček M., Vaněk M.: *Use of Welding Process Numerical Analyses as Technical Support in Industry. Part 2: Methodology and Validation*. Biuletyn Instytutu Spawalnictwa, 2015, no. 5, pp. 25-32. <http://dx.doi.org/10.17729/ebis.2015.5/4>
- [3] Slováček M., Kik T.: *Use of Welding Process Numerical Analyses as Technical Support in Industry. Part 3: Industrial Examples - Transport Industry*. Biuletyn Instytutu Spawalnictwa, 2015, no. 6, pp. 38-45. <http://dx.doi.org/10.17729/ebis.2015.6/5>
- [4] Chukkan J. R., Vasudevan M., Muthukumar S., Ravi Kumar R., Chandrasekhar N.: *Simulation of laser butt welding of AISI 316L stainless steel sheet using various heat sources and experimental validation*. Journal of Materials Processing Technology, 2015, vol. 219, pp. 48-59. <http://dx.doi.org/10.1016/j.jmatprotec.2014.12.008>
- [5] Tsirkas S.A., Papanikos P., Kermanidis Th.: *Numerical simulation of the laser welding process in butt-joint specimens*. Journal of Materials Processing Technology, 2003, vol. 134, no. 1, pp. 59-69. [http://dx.doi.org/10.1016/S0924-0136\(02\)00921-4](http://dx.doi.org/10.1016/S0924-0136(02)00921-4)
- [6] Seang C., David A.K., Ragneau E.: *Nd:YAG Laser Welding of Sheet Metal Assembly: Transformation Induced Volume Strain Effect on Elastoplastic Model*. Physics Procedia, 2013, vol. 41, pp. 448-459. <http://dx.doi.org/10.1016/j.phpro.2013.03.101>
- [7] Piekarska W., Kubiak M., *Modelling of thermal phenomena in single laser beam and laser-arc hybrid welding processes using*

- projection method*, Applied Mathematical Modelling 37, 4, 2013, pp. 2051–2062.
<http://dx.doi.org/10.1016/j.apm.2012.04.052>
- [8] Piekarska W., Kubiak M.: *Comprehensive model of thermal phenomena and phase transformations in laser welding process*. Computers & Structures, 2016, vol. 172, pp. 29–39.
<http://dx.doi.org/10.1016/j.compstruc.2016.05.014>
- [9] SYSWELD material database
- [10] Joshi S., Hildebrand J., Abdulkareem S. Aloraier, Rabczuk T.: *Characterization of material properties and heat source parameters in welding simulation of two overlapping beads on a substrate plate*. Computational Materials Science, 2013, vol. 69, pp. 559–565.
<http://dx.doi.org/10.1016/j.commatsci.2012.11.029>
- [11] SYSWORLD 2013 Technical Description of Capabilities.
- [12] Majchrzak E.: *Wykłady: Przepływ ciepła – konwekcja, Przepływ ciepła – promieniowanie*. Instytut Mechaniki i Inżynierii Obliczeniowej, Wydział Mechaniczny Technologiczny, Politechnika Śląska.
- [13] MHTL Simulation Tools. access date: 28.09.2016.
www.mhtl.uwaterloo.ca/RScalculators.html
- [14] Han L., Liou F.W.: *Numerical investigation of the influence of laser beam mode on melt pool*. International Journal of Heat and Mass Transfer, 2004, vol. 47, no. 19-20, pp. 4385-4402.
<http://dx.doi.org/10.1016/j.ijheatmasstransfer.2004.04.036>
- [15] Abderrazak K., Bannour S., Mhiri H., Lepalec G., Autric M.: *Numerical and experimental study of molten pool formation during continuous laser welding of AZ91 magnesium alloy*. Computational Materials Science, 2009, vol. 44, no. 3, pp. 858-866.
<http://dx.doi.org/10.1016/j.commatsci.2008.06.002>
- [16] Melting temperature ranges for stainless steels. access date: 28.09.2016.
www.bssa.org.uk/topics.php?article=103